Since January 2020 Elsevier has created a COVID-19 resource centre with free information in English and Mandarin on the novel coronavirus COVID-19. The COVID-19 resource centre is hosted on Elsevier Connect, the company's public news and information website.

Informatics in Medicine Unlocked 24 (2021) 100569

Contents lists available at ScienceDirect

Informatics in Medicine Unlocked

journal homepage: http://www.elsevier.com/locate/imu

Computational prediction of potential siRNA and human miRNA sequences to silence orf1ab associated genes for future therapeutics against SARS-CoV-2

Mahedi Hasan, Arafat Islam Ashik, Md Belal Chowdhury, Atiya Tahira Tasnim, Zakia Sultana Nishat, Tanvir Hossain, Shamim Ahmed *

Department of Biochemistry and Molecular Biology, Shahjalal University of Science and Technology, Sylhet 3114, Bangladesh

A R T I C L E I N F O

Keywords:
RNAi Therapeutics
Gene silencing
miRNA
siRNA
COVID-19
SARS-CoV-2
Posttranscriptional regulation

A B S T R A C T

The coronavirus disease 2019 (COVID-19) is an ongoing pandemic caused by an RNA virus termed as severe acute respiratory syndrome coronavirus-2 (SARS-CoV-2). SARS-CoV-2 possesses an almost 30kbp long genome. The genome contains open-reading frame 1ab (ORF1ab) gene, the largest one of SARS-CoV-2, encoding polyprotein PP1ab and PP1a responsible for viral transcription and replication. Several vaccines have already been approved by the respective authorities over the world to develop herd immunity among the population. In consonance with this effort, RNA interference (RNAi) technology holds the possibility to strengthen the fight against this virus. Here, we have implemented a computational approach to predict potential short interfering RNAs including small interfering RNAs (siRNAs) and microRNAs (miRNAs), which are presumed to be intrinsically active against SARS-CoV-2. In doing so, we have screened miRNA library and siRNA library targeting the ORF1ab gene. We predicted the potential miRNA and siRNA candidate molecules utilizing an array of bioinformatic tools. By extending the analysis, out of 24 potential pre-miRNA hairpins and 131 siRNAs, 12 human miRNA and 10 siRNA molecules were sorted as potential therapeutic agents against SARS-CoV-2 based on their GC content, melting temperature (T_m), heat capacity (C_p), hybridization and minimal free energy (MFE) of hybridization. This computational study is focused on lessening the extensive time and labor needed in conventional trial and error based wet lab methods and it has the potential to act as a decent base for future researchers to develop a successful RNAi therapeutic.

1. Introduction

SARS-CoV-2 is a positive single-stranded RNA virus that has been ailing millions of human beings around the world since December 2019. The disease COVID-19 caused by this virus, ultimately leads to respiratory failure and then progresses up to multiple organ failure [1,2]. Due to the higher transmission rate, the virus has spread out whole over the world resulting in massive break out of COVID-19 disease and subsequently, COVID-19 was declared as a global pandemic [3]. Since the first report of a cluster of patients in Wuhan city of China, this virus has already claimed the lives of more than 2 million people around the world and the number is still increasing day by day [4]. To terminate this global pandemic, researchers are now in the race against time to develop vaccines and antiviral drugs. Their efforts are being challenged by the frequent mutation of the virus that has resulted in variants with higher transmission rates [5]. There are also instances of and reported the ineffectiveness of some approved vaccines against new variants [6–8].

There are several variants of SARS-CoV-2 and all the variants share common fundamental features. The virus has been classified under the *Coronaviridae* family with almost 30 kb long (+) ssRNA genome and there are four major types of structural proteins that construct the capsid [9]. During the initiation stage of infection, SARS-CoV-2 launches its spike glycoprotein (S protein) onto the angiotensin converting enzyme 2

Abbreviations: SARS-CoV-2, severe acute respiratory syndrome coronavirus-2; COVID-19, coronavirus disease 2019; ACE-2, Angiotensin-converting enzyme 2; ORF, open reading frame; RNAi, RNA interference; miRNA, microRNA; siRNA, small interfering RNA; T_m, melting temperature; C_p, heat capacity; TMPRSS2, transmembrane protease serine 2; sgRNA, sub-genomic RNA; UTR, untranslated region; hsa-miR, human microRNA.

* Corresponding author.
E-mail addresses: shamim1174-bmb@sust.edu, shamim1174@gmail.com (S. Ahmed).

https://doi.org/10.1016/j.imu.2021.100569
Received 17 December 2020; Received in revised form 26 March 2021; Accepted 31 March 2021
Available online 8 April 2021

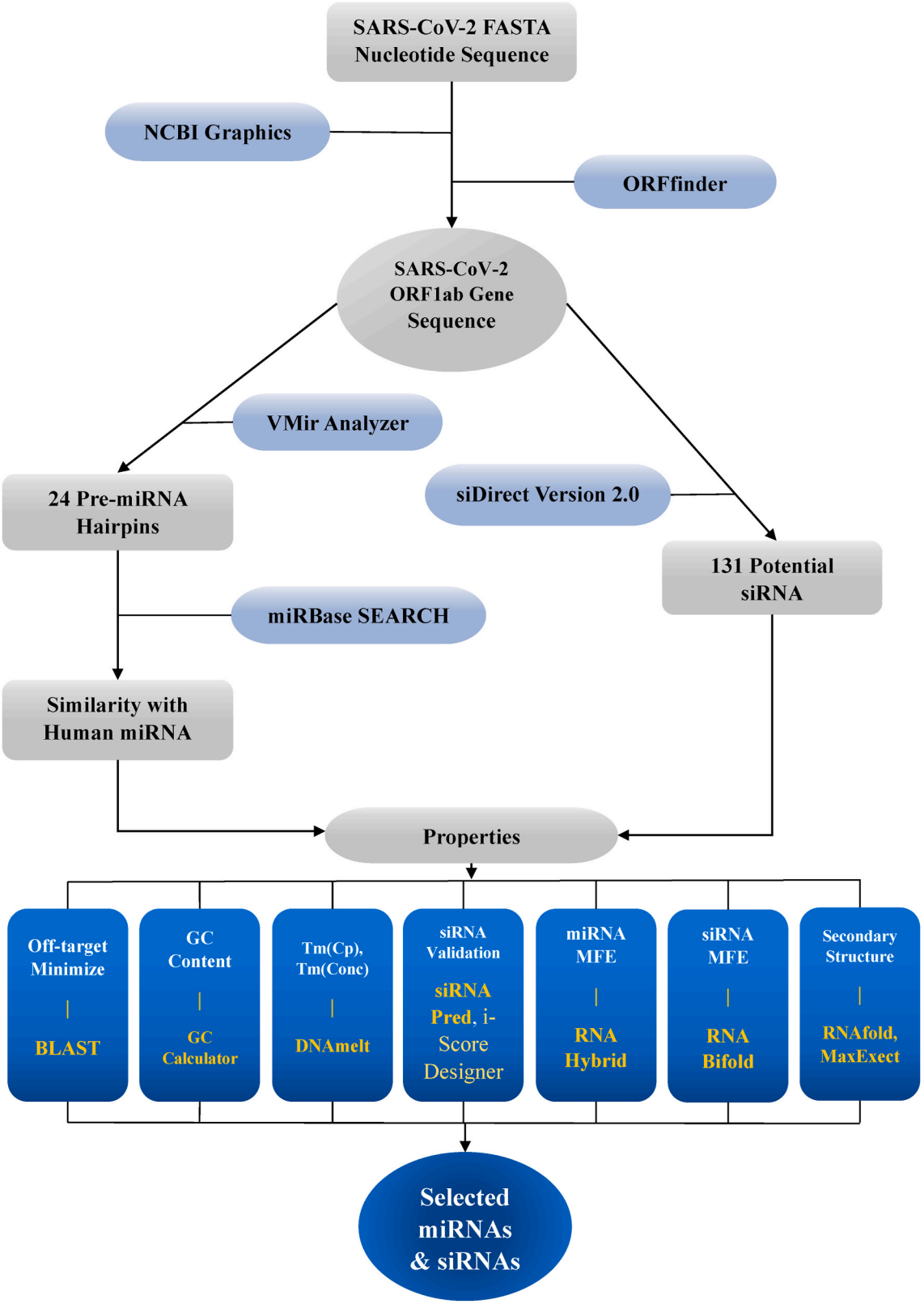

Fig. 1. Flow diagram of entire steps. Graphical representation of complete processes which has been taken in this study are summarized.

(ACE-2) receptor, mostly abundant in the lungs and airways in the human body. Enzymes like furin or transmembrane protease serine 2 (TMPRSS2), found on the exterior surface of the host cells, cleaves the S protein in several specific sites to expose the fusion peptides that help the SARS-CoV-2 membrane to fuse with the host cell membrane. This fusion allows the RNA genome of SARS-CoV-2 to gain entry into the host cell [10]. The replication-transcription complex (RTC) of SARS-CoV-2 transcribes the viral negative-stranded sub-genomic RNAs (sgRNAs) that translate the structural and nonstructural accessory proteins. In all coronavirus genome, including the one of SARS-CoV-2, the 3′-terminus

ORFs encode the structural proteins such as, S proteins, envelope proteins (E), membrane proteins (M), and nucleocapsid proteins (N) [11]. The 5′ terminus ORF1ab region (21,291 nucleotides long) contains overlapping open reading frames that encode polyproteins PP1ab and PP1a. Both of these polyproteins act as precursor for 16 non-structural proteins (nsp 1 to 16) [9] and in addition to that these two have major role in viral replication, transcription, immune response modulation [12,13]. Because of the vital functions of these proteins, the corresponding genes of pp1ab and pp1a silencing can downregulate the overall expression of all the genomic and replicator components of SARS-CoV-2. Thus, ORF1ab could be a target for RNAi-mediated gene silencing.

RNAi is the sequence specific post-transcriptional gene silencing mechanism mediated by double-stranded RNAs (dsRNAs), either endogenous pre-miRNA precursors or exogenous longer siRNAs [14,15]. Thus, dsRNAs could be exploited as the degrader of homologous mRNA of a viral gene [16–18]. Consequently, viral activity can also be controlled by RNAi technology. RNAi mechanism initiates with the cleaving of dsRNAs by RNase-III like protein Dicer resulting in shorter 21–25 nucleotides interfering RNAs with 2–3 nucleotides overhangs [19]. The resulted shorter interfering RNAs are subsequently incorporated into the RNA-induced silencing complex (RISC) [20]. Unwinding of the shorter dsRNAs mediated by an RNAi-associated helicase causes the loss of one strand (passenger strand) [21]. The other strand (guide strand) of RNAi (miRNA or siRNA) directs RISC-mediated recognition and cleavage of the target mRNA (complementary to the viral antisense strand) [22–24].

The miRNAs are encoded in higher eukaryotes genome and regulate gene expression at post-transcriptional level. In general, RNA polymerase II transcribes the long hairpin structured primary miRNA (pri-miRNA). DGCR8 (a dsRNA binding protein) and Drosha (RNase III protein) microprocessor complex excise the pri-miRNA to make precursor miRNA (pre-miRNA). Pre-miRNA is respectively exported to the cytoplasm by exportin protein and cleaved by RNase III type Dicer protein to become short double-stranded miRNA. The processed miRNA antisense guide strand is then recognized by RISC and binds the partial complementary target mRNA. The partial binding of miRNA guide strand with mRNA leads to the translational repression by inhibiting ribosome and sometimes leads to mRNA degradation with the help of RISC Argonaute protein [25]. Whereas, siRNAs are defenders of genomic integrity and response against exogenous invasive nucleic acids, such as viral genomes [26]. siRNAs are exogenous in nature or experimentally designed to regulate the gene expression at the post-transcriptional level by introducing long non-coding double-stranded RNA in the cytoplasm with the help of nanoparticle vectors [27]. After being introduced into the cell, siRNA is cleaved by RNase III type Dicer protein to become short double-stranded siRNA. And by the similar mechanism of miRNA, siRNA also binds to the complementary mRNA. Unlike miRNA, a perfect complementarity between siRNA guide strand and target mRNA is crucial to warrant degradation of the mRNA by the Argonaute protein of RISC [28].

In some recent studies, miRNAs and siRNAs have been explored as an antiviral defense against several viruses, including human immunodeficiency virus-1 (HIV-1) [29–31], Dengue [32,33], Influenza [34–36], Hepatitis C (HCV) [37–39], and Zika [40]. In 2018, a siRNA drug (Patisiran) was approved by the U.S. Food and Drug Administration (FDA) [41]. The use of miRNAs as an anti-HCV treatment demonstrates promising efficacy and safety results in an early-stage trial [37], and it shouldn't be overlooked that siRNA has already been applied against hepatitis B infection [42]. Therefore, it is presumable that RNAi therapeutics will be able to effectively inactivate the mRNA of SARS-CoV-2 in a sequence-specific manner and hence can work as potential antiviral therapeutics [41].

As the precarious situation of the disease COVID-19 has stipulated the search for different alternative solutions to conjunctly fight the virus and thus the development of effective therapeutic have come into play. Harnessing RNAi technology-based therapeutics against COVID-19 holds the potential to act target specifically and effectively [43,44]. In the present study, the SARS-CoV-2 viral genome was scanned to identify potential siRNA and cellular miRNA molecules for the silencing of the ORF1ab coding mRNAs using computational approaches. Computational approach undertaken in this study employed ORF1ab coding mRNAs of SARS-CoV-2 to predict miRNA and siRNA as antivirals against it. Candidate miRNA was screened by a prediction platform VMir which predicts pre-miRNA from any given viral genome completely by ab-initio method [45]. Alongside miRNA, siRNA from the viral genome sequence was identified by siDirect program (http://sidirect2.rnai.jp/) that implements fast and sensitive homology search algorithm to ensure functional and off-target minimized siRNA design for mammalian RNAi [46,47]. Few best siRNA and miRNA molecules were sorted based on different parameters, such as GC content, free energy of folding, free energy of binding, melting temperature, efficacy prediction from the primarily found candidate RNAi molecules (Fig. 1).

The extent of the damage by COVID-19 is increasing day by day. The predicted siRNA and human miRNA from the analyses will be capable of contribute to the fight against SARS-CoV-2. Also, for the available insertion techniques, specificity, and cost-effectiveness [48], RNAi is going to be the next generation therapeutics, and hence, this study may provide a benchmark for the establishment of RNAi therapeutics against SARS-CoV-2 as an effective treatment for COVID-19.

2. Materials and methods

2.1. Sequence acquisition and analysis

The RNAi prediction against SARS-CoV-2 was carried out using the nucleotide sequence (GB: NC_045512.2) obtained from the database of National Center for Biotechnology Information (NCBI). For the "ORF1ab" gene, NCBI graphics database was used to acquire the nucleotide sequence of 266-21,555 bp (https://www.ncbi.nlm.nih.gov/nuccore/NC_045512.2?report=graph). After retrieving the ORF1ab gene sequence, BLAST (Basic Local Alignment Search Tool) (https://blast.ncbi.nlm.nih.gov/Blast.cgi) was used to observe sequence similarities among all the available SARS-CoV-2 strains around the world available in GenBank, the National Institutes of Health (NIH) genetic sequence database. An online tool, the ORF finder was utilized to screen the coding regions in the retrieved ORF1ab gene from our reference sequence.

2.2. Potential miRNA and siRNA designing

The nucleotide sequence of the ORF1ab gene of the SARS-CoV-2 viral genome was scrutinized for hairpin-structured miRNA precursors using a VMir Analyzer program [49,50]. VMir is an analyzing program that is specifically designed to identify hairpin-structured pre-miRNA in the viral genome. By VMir viewer, potential hairpin-like structures as candidate miRNA precursors were visualized. To get bona fide pre-miRNA from VMir, custom setting cut-off value of 60 nucleotides minimum, 220 nucleotides maximum, and 115 minimum hairpin score [51] was used. The candidate hairpin miRNA sequences extracted from VMir were screened for sequence similarity with all human microRNAs by applying the SEARCH method of miRBase [52,53], a searchable database of published miRNAs. Sequence homology between viral pre-miRNA hairpin with human miRNA was retrieved by using BLASTN search algorithm in miRBase database with E-value 10.

siDirect version 2.0 [54], an online web server to design siRNA, was used to predict possible siRNAs for target gene ORF1ab. This updated web-server uses a fast, sensitive homology search algorithm to ensure functional and off-target minimized siRNA design for mammalian RNAi. Several parameters were marked in the siDirect site to get potential siRNAs, including melting temperature below 21.5 °C, GC content 31.6%–57.9% [55,56] and Ui-Tei [57,58], Renold [59], Amarzguioui

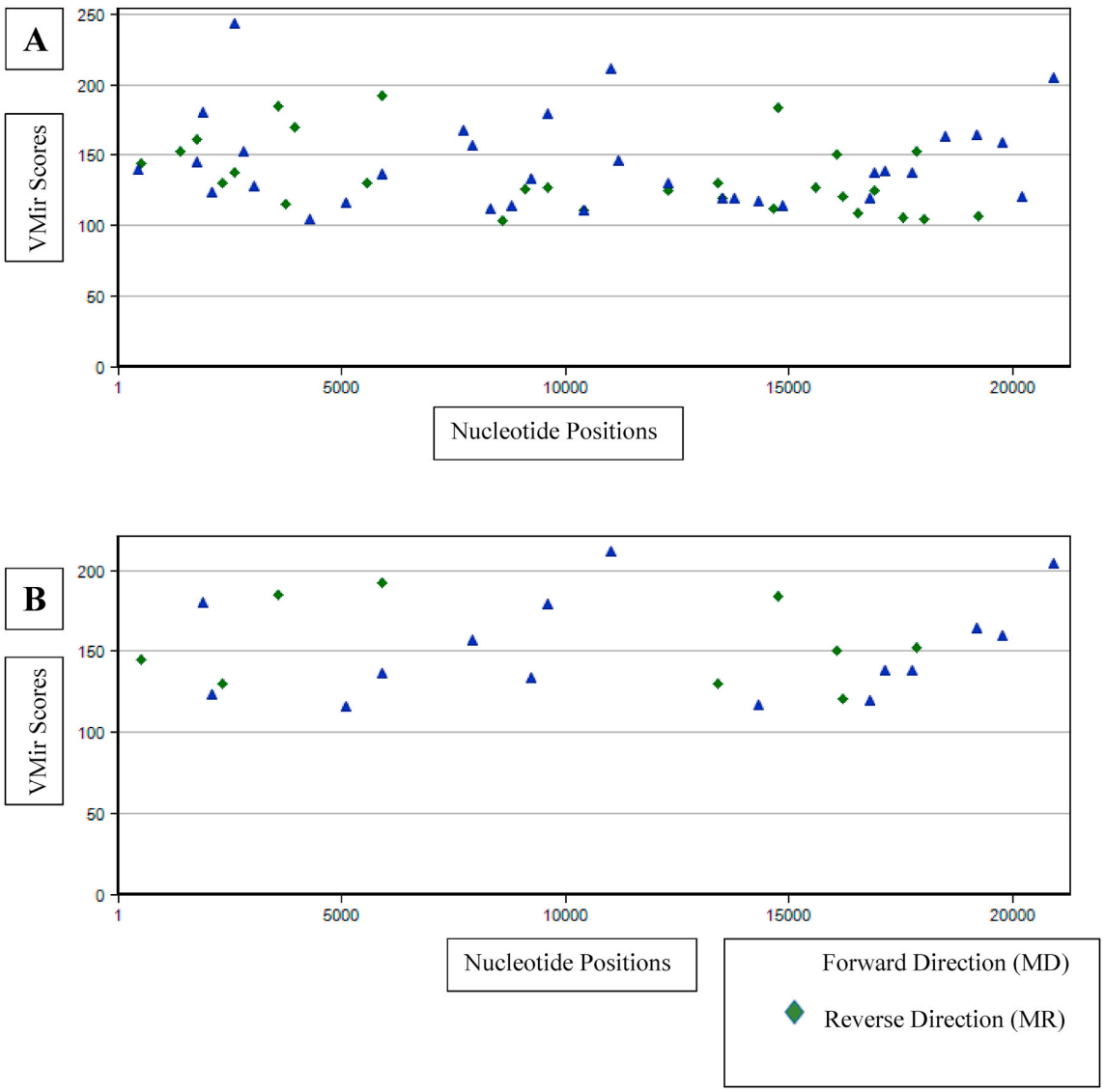

Fig. 2. Graphical view of VMir analysis of the SARS-CoV-2 genome. A. Default B. Predicted pre-miRNA after filtering (minimum hairpin size: 60 nt, maximum hairpin size: 120 nt, minimum hairpin score: 115, and minimum window count:25). The blue triangle shape refers to forward direction and green diamond shape are reverse direction precursor hairpins. (For interpretation of the references to colour in this figure legend, the reader is referred to the Web version of this article.)

[55] combined rules (algorithms have given in Supplementary Table S1). And the seed-target duplex stability (T_m) was calculated, which is for the formation of the RNA duplex.

2.3. Off-target minimization and GC content calculation

Nucleotide BLAST (BLASTn) program was operated for siRNA against the human genomic plus transcript database using default parameters, to check off-target sequences in the genome of any non-targeted sites. Consequently, a web-based server, GC Content Calculator (http://www.endmemo.com/bio/gc.php), was utilized to calculate the exact percentages of GC content in predicted siRNA and miRNA.

2.4. Calculation of heat capacity and concentration plot of RNA-duplex

The collective heat capacity of RNA-duplex is denoted as C_p, and after it is plotted as a function of temperature, the melting temperature, T_mC_p is the local maximum of heat capacity curve. Using the inclusive heat capacity plot where melting temperature T_m(Conc), indicates the temperature at which the concentration of double-stranded molecule becomes one-half of its maximum value. For both miRNA and siRNA, the T_mC_p and T_m(Conc) were measured using the DNAmelt Server [60,61], including Hybridization of two different strands option (http://unafold.rna.albany.edu/?q=DINAMelt/Hybrid2), with default values and in simple form marking RNA option. The heat capacity graph was plotted by the server based on the numerical differentiation calculation of the ensembled free energy profiles with respect to temperature.

2.5. Hybridization and secondary structure prediction of miRNA

An online free accessible RNA hybrid web server [62,63] was used to predict the hybridization and calculated the minimum free energy (MFE) of hybridization between the viral precursor miRNAs and complementary template of the potential human miRNAs. For the selection of potential miRNA, the energy threshold value at −10 kcal/mol was utilized as a cut-off score. The result of RNA hybrid was categorized in terms of pairing energy (MFE). RNAfold is another webserver (http://rna.tbi.univie.ac.at/cgi-bin/RNAfold.cgi) that predicts the secondary structures of single-stranded RNA or DNA sequences, and it was operated to predict the most stable secondary structure of selected miRNA hairpin sequences. Two types of hybridization patterns were obtained from RNA fold – MFE and Centroid. This web server has validated results

Table 1
Alignments of precursor miRNAs hairpin sequences with human miRNAs, corresponding VMir score, E-value, T_mC_p and T_m (**Conc**) .

Hairpin	Score	Alignments between SARS-CoV-2 and human miRNA	E-value	T_mC_p °C	T_m(conc) °C
MD7	180.1	UserSeq 77 gaguuucuuagagacg 92 hsa-miR-3675-3p 16 gaguuccuuagagaug 1	9.6	66.8	64.4
MD18	135	UserSeq 25 accugcucuacaagaugcuu 44 hsa-miR-492 4 accugcgggacaagauucuu 23	7.3	63	64.5
MD23	136.3	UserSeq 17 acuuaaauggugaugugguggcu 39 hsa-miR-302a-5p 1 acuuaaacguggauguacuugcu 23	9.5	56.8	61.9
MD42	211.4	UserSeq 34 gauaugguugauacuaguuug 54 hsa-miR-190b-5p 2 gauauguuugauauuggguug 22	2.3	55.8	60.7
MD55	119.8	UserSeq 51 aagagucauuuugcuauuggcc 72 hsa-miR-548b-5p 1 aaaaguaauugugguuuuggcc 22	5.2	60.7	64.6
		UserSeq 34 gaccaccugguacuggua 51 hsa-miR-624-5p 21 gaacacaagguacuggua 4	7.6	68.3	65.5
		UserSeq 29 ccagggaccaccuggu 44 hsa-miR-4640-5p 5 ccagggagcagcuggu 20	9.2	87.8	79.6
MD64	164.8	UserSeq 30 cguguauaacacguugcaauuu 51 hsa-miR-363-5p 1 cggguggaucacgaugcaauuu 22	4.7	72.4	71.3
MD66	159.3	UserSeq 62 uuaaagguuuacaaccau 79 hsa-miR-4802-3p 21 uugaagguuuccauccau 4	8.6	67.5	65.6
MD70	204.7	UserSeq 50 uucuuggaaugcugaucu 67 hsa-miR-23b-5p 5 uuccuggcaugcugauuu 22	8.2	64.7	61.2
MR11	185.1	UserSeq 46 uucaacuugcuuuucacucu 65 hsa-miR-5586-3p 21 uuuaaccagcuugucacucu 2	8.7	44.3	51.7
MR33	183.9	UserSeq 60 aaagugcaucuugauccuc 78 hsa-miR-363-5p 22 aaauugcaucgugauccac 4	3.1	44.3	51.7
MR38	150.4	UserSeq 37 uaauuuaugugauguug 53 hsa-miR-153-5p 1 ucauuuuugugauguug 17	3.9	55.6	53.2
MR43	152.7	UserSeq 82 ugccuguguaggaugu 97 hsa-miR-448 2 ugcauauguaggaugu 17	8.9	57.8	60.4
		UserSeq 66 cacugaggugugaggug 83 hsa-miR-4420 3 cacugaugucuguagcug 20	7.4	57.5	56.4
		UserSeq 50 uugaauuuagugucaaca 67 hsa-miR-744-3p 19 uugagguuaguggcaaca 2	7.4	59.6	61.6

based on generated ensemble diversity and similarity between MFE and Centroid model.

2.6. Validation of predicted siRNA molecules

To check the validation and the actual efficacy of the siRNA molecules, an online free accessible server siRNApred (http://crdd.osdd.net/raghava/sirnapred/**)** was employed. In this method, the siRNA molecules were screened against the Main21 dataset using the support vector machine algorithm and the binary pattern prediction approach. To assess the extent of validity, along with the siRNApred, the i-Score Designer tool [64] was also used to check the predicted siRNA molecules based on second generation algorithm that calculates i-score and s-Biopredsi scores.

2.7. Secondary structure prediction and RNA-RNA interaction of siRNA

The secondary structure of siRNAs was predicted along with the respective free energy of folding using the MaxExpect [65] program in the RNA structure web server [66]. Here, guide strands of predicted siRNAs were subjected to RNA structure web. In MaxExpect program, nucleic acid sequence must not be longer than 4000 nucleotides whereas other parameters remained with default value. This server uses SHAPE mapping data for folding. Afterwards, to calculate thermodynamics interaction between the viral siRNAs and the target sequences, the RNA structure web server, containing the bifold section (http://rna.urmc.rochester.edu/RNAstructureWeb/Servers/bifold/bifold.html) was utilized. Both sequences were no longer than 250 nucleotide which was one of the prerequisites of bifold section of this server. Other parameters such maximum percent of energy difference and temperature kept in its default values.

3. Result

3.1. Potential precursor miRNA predicted by VMir

ORF1ab gene covers the two-thirds length of the whole genome of SARS-CoV-2, and it is the first line open reading frame gene that contains

Table 2
Energetically favorable hybridization between microRNA and viral large hairpin RNA, GC% and minimum free energy (MFE) binding with target.

Hairpin	Hairpin Sequence	GC %	Most favorable hybridization sites of a miRNA in a large hairpin of viral RNA	MFE (kcal/mol)
MD7	TAACATCTTTGGCACTGTTTATG AAAAACTCAAACCCGTCCTTGAT TGGCTTGAAGAGAAGTTTAAGG AAGGTGTAGAGTTTCTTAGAGAC GGTTGGGAAATTGTTA	38.32	target 5' A U A 3' GUUUCU AG GAC UAGAGA UC UUG miRNA 3' U C AG 5'	-11.3
MD18	ACAAATAGAGTTGAAGTTTAATC CACCTGCTCTACAAGATGCTTAT TACAGAGCAAGGGCTGGTGAAG CTGCTAACTTTTGTG	40.96	target 5' A U 3' CCUGC GGGCG miRNA 3' UCUUAGAACA UCCA 5'	-13.0
MD55	AGGTTGGTATGCAAAAGTATTCT ACACTCCAGGGACCACCTGGTAC TGGTAAGAGTCATTTTGCTATTG GCCT	45.21	target 5' A U A 3' AGAGUCAU UUGCU UUUUGGUG AAUGA miRNA 3' CGG UU AAA 5'	-12.0
			target 5' C U G 3' ACC GGUACU GU UGG UCAUGG CA miRNA 3' A AACA AG 5'	-15.3
			target 5' G ACCA 3' CCAG G CCUGG GGUC C GGACC miRNA 3' GA GAG 5'	-17.2
MD64	TATAGATTATGTACCACTAAAGT CTGCTACGTGTATAACACGTTGC AATTTAGGTGGTGCTGTCTGTA	38.24	target 5' UAUAA G 3' CGUG CAC GCAC GUG miRNA 3' UUAACGUA UAG GGC 5'	-12.7
MD66	GATGGTCAAGTAGACTTATTTAG AAATGCCCGTAATGGTGTTCTTA TTACAGAAGGTAGTGTTAAAGGT TTACAACCATC	36.25	target 5' A UUUAC A 3' GG AACC CC UUGG miRNA 3' A UACCU AAGUU 5'	-11.0
MD70	AACAAAAGCTAGCTCTTGGAGG TTCCGTGGCTATAAAGATAACAG AACATTCTTGGAATGCTGATCTT TATAAGCTCATGGGACACTTCGC ATGGTGGACAGCCTTTGTT	42.73	target 5' C A G 3' UUGG AUGCU AGUC UACGG miRNA 3' UU G UCCUU 5'	-12.3
MR33	GGCATACTTAAGATTCATTTGAG TTATAGTAGGGATGACATTACGT TTTGTATATGCGAAAAGTGCATC TTGATCCTCATAACTCATTGAAT CATAATAAAGTCTAGCC	33.94	target 5' A U 3' GUGCA UACGU miRNA 3' ACCUAGUGC UAAA 5'	-10.2
MR43	GGTCATGTCCTTAGGTATGCCAG GTATGTCAACACATAAACCTTCA GTTTTGAATTTAGTGTCAACACT GAGGTGTGTAGGTGCCTGTGTAG GATGTAACC	43.56	target 5' C G 3' UGC UGUGUA AUG AUACGU miRNA 3' GUAGG U 5'	-12.0
			target 5' C U G GU A 3' AC GA GU GU UG CU UA CA miRNA 3' UCGA U G GU C 5'	-13.1
			target 5' AAU UG C 3' UUG UUAG UCAA AAC GAUU AGUU miRNA 3' C GGU GG 5'	-10.3

all the important coding regions. The analysis showed 99.99% similarities of ORF1ab gene sequences among all SARS-CoV-2 strains available in GenBank after using BLAST. Therefore, designing the miRNA and siRNA using the conserved sequence will be of broader efficacy.

ORF1ab gene was scrutinized for hairpin-structured miRNA precursors using a VMir Analyzer program and candidate miRNA precursors were visualized graphically with score length and score by VMir Viewer. In the default setting, 61 candidate hairpins were found that are shown in Fig. 2A. By using custom settings, 24 potential pre-miRNA hairpins were found for further analyses, which is illustrated in Fig. 2B.

3.2. Identical human miRNAs predicted from precursor pre-miRNA by miRBase

The sequences of candidate precursors of pre-miRNAs were searched for nucleotide similarity with all human miRNAs by miRBase online server. Based on significant sequence similarity, 12 sequences were identified as candidate miRNA precursors [SUPPLEMENTARY TABLE S2], which showed a minimum of 16 bp similarity with human miRNAs. Precursors of pre-miRNAs were differentiated by forward direction (MD) and reverse direction (MR). All the 12 pre-miRNA precursors were MD7, MD18, MD23, MD42, MD55, MD64, MD66, MD70, MR11, MR33, MR38, and MR 43 had shown approximate identity with 16 human miRNAs (Table 1).

3.3. siRNA prediction with siDirect

Several parameters were marked in the siDirect site to get potential siRNAs. The parameter includes Ui-Tei, Renold, Amarzguioui combined rules, GC content from 31.6% to 57.9%, melting temperature below 21.5 °C to reduce the seed-dependent off-target effect. Based on these mentioned parameters from the siDirect site, 131 potential siRNAs were found (Supplementary Table S2). Using the nearest-neighbor model and the thermodynamic parameters for the formation of siRNA duplex, the seed-target duplex was also predicted, and all the siRNA duplexes were observed to have the T_m value below 21.5 °C (Supplementary Table S3).

3.4. Significant GC content of miRNAs and siRNAs with off-target minimization of siRNAs

The exact percentages of GC content in predicted miRNA molecules and siRNA molecules were calculated through GC Content Calculator.

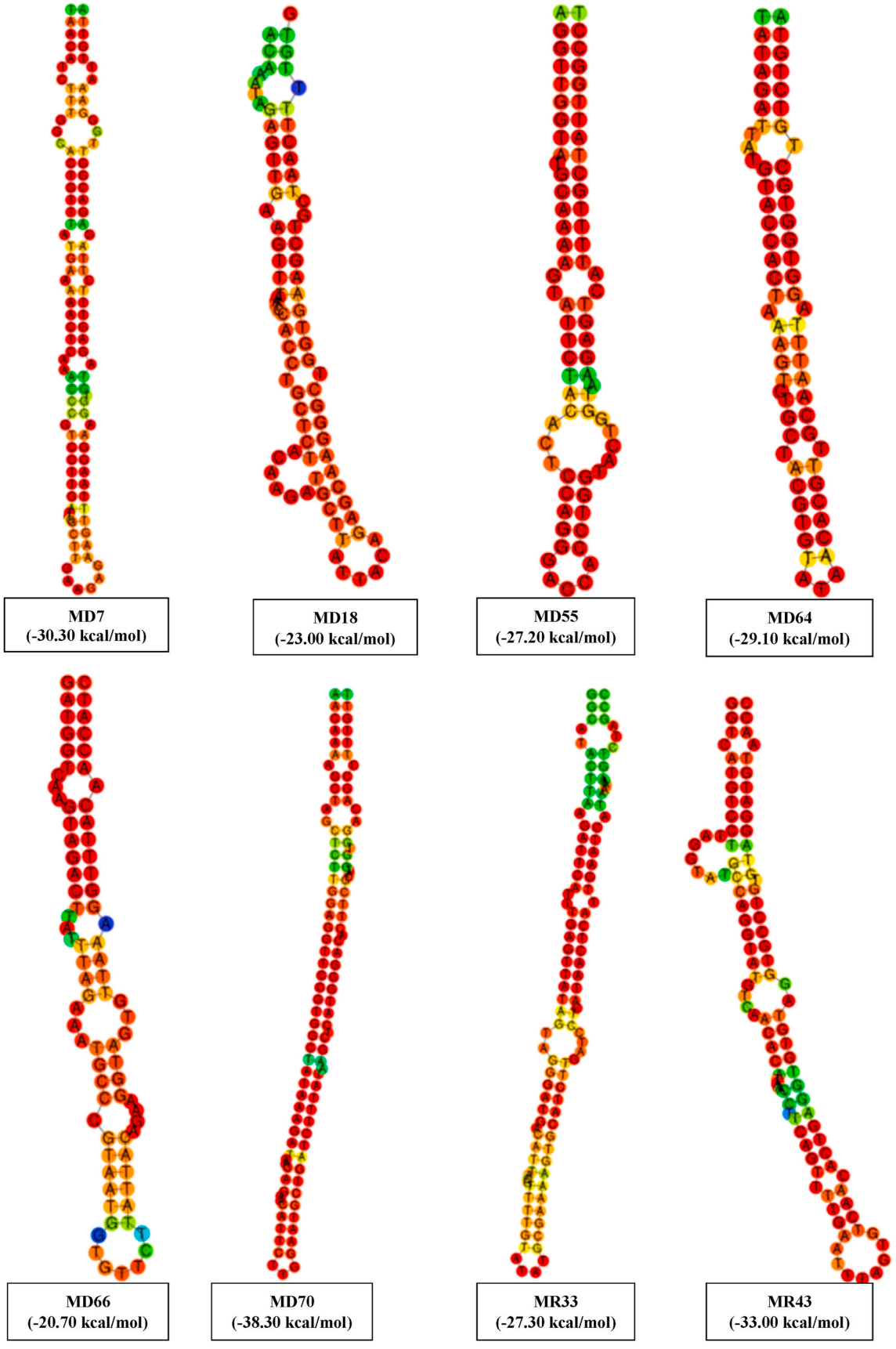

Fig. 3. Predicated secondary structure of potential hairpins candidate of SARS-CoV-2. Only centroid structures are depicted.

Table 3
Effective siRNA molecule with GC%, free energy of binding (MEF) with target, T_mC_p, T_m (Conc), validity (binary), s-Biopredsi score, and i-Score.

Alias	Location of target within mRNA	siRNA target within mRNA	Predicted siRNA duplex siRNA candidate at 37 °C	GC% (%)	MFE (kcal/mol)	T_mC_p °C	T_m(conc) °C	Validity (binary)	s-Biopredsi score	i-Score
s1	3051–3073	ACCAGTTGTTCAGACTATTGAAG	UCAAUAGUCUGAACAACUGGU CAGUUGUUCAGACUAUUGAAG	38.1	−34.80	81.4	80.7	1.008	0.830	66.9
s2	3136–3158	GTGGAAGAAGCTAAAAAGGTAAA	UACCUUUUUAGCUUCUUCCAC GGAAGAAGCUAAAAAGGUAAA	38.1	−33.90	83	81.6	1.062	0.863	84.4
s3	3318–3340	CGGACACAATCTTGCTAAACACT	UGUUUAGCAAGAUUGUGUCCG GACACAAUCUUGCUAAACACU	42.86	−35.00	83.1	81.9	1.072	0.807	67.3
s4	3869–3891	TTGTTCAAGAGGGTGTTTTAACT	UUAAAACACCCUCUUGAACAA GUUCAAGAGGGUGUUUUAACU	33.33	−31.50	82.5	81.3	1.031	0.781	66.8
s5	8981–9003	CTGGTGTTTGTGTATCTACTAGT	UAGUAGAUACACAAACACCAG GGUGUUUGUGUAUCUACUAGU	38.1	−34.40	82.6	81.2	1.001	0.873	78.8
s6	9002–9024	GTGGTAGATGGGTACTTAACAAT	UGUUAAGUACCCAUCUACCAC GGUAGAUGGGUACUUAACAAU	42.86	−36.80	84.7	83.4	1.024	0.762	69.7
s7	11664–11686	GGCTCAATGTGTCCAGTTACACA	UGUAACUGGACACAUUGAGCC CUCAAUGUGUCCAGUUACACA	47.62	−38.40	84.9	83.8	1.003	0.643	62.7
s8	13404–13426	TTCTCTAACTACCAACATGAAGA	UUCAUGUUGGUAGUUAGAGAA CUCUAACUACCAACAUGAAGA	33.33	−32.70	81.2	79.9	1.018	0.832	71.3
s9	17690–17712	TTGCATAATGTCTGATAGAGACC	UCUCUAUCAGACAUUAUGCAA GCAUAAUGUCUGAUAGAGACC	33.33	−33.00	80.2	79.3	1.049	0.838	72.1
s10	18338–18360	TGGCTTTGAGTTGACATCTATGA	AUAGAUGUCAACUCAAAGCCA GCUUUGAGUUGACAUCUAUGA	38.1	−34.80	83.3	82.1	1.037	0.849	75.9

The resultant GC content for miRNAs and siRNAs were respectively from 33.94% to 45.21% (Table 2) and 33.33%–47.62% (Supplementary Table S2). Also, the off-target for predicted siRNA was less than the other siRNAs, and there was no significant sequence similarity with the human genomic and transcript sequence database that made them much effective for only the targeted sites.

3.5. Higher effectiveness of miRNAs and siRNAs according to heat capacity and RNA-duplex concentration

Using the DNAmelt Server, T_mC_p and T_m(Conc) for both miRNAs and siRNAs were measured. The higher values of these two melting temperatures indicate the higher effectiveness of the RNAi species. T_mC_p and T_m(Conc) values ranged from 43 °C to 87.8 °C and from 40.4 °C to 79.6 °C respectively for miRNAs (Table 1). Similarly, T_mC_p and T_m(Conc) values of siRNAs ranged from 79.6 °C to 87.6 °C and from 78.2 °C to 86.3 °C respectively (Supplementary Table S2).

3.6. Hybridization and secondary structure prediction of miRNAs

RNA hybrid web server [63] was utilized to display significant hybridization between potential viral precursor miRNAs and complementary templates of the potential human miRNAs. Their corresponding minimal free energy of hybridization is given in Table 2. The minimal free energy of hybridization was ranged from −10 kcal/mol to −17.2 kcal/mol. RNAfold was used to predict the secondary RNA structure of predicted miRNAs that are presented in Fig. 3. Later based on significant sequence similarity, hybridization, and all other parameters, 12 potential cellular miRNAs were predicted targeting the SARS-CoV-2. All the predicted human miRNAs are hsa-miR-3675–3p, hsa-miR-492, hsa--miR-548b-5p, hsa-miR-624–5p, hsa-miR-4640–5p, hsa-miR-363–5p, hsa-miR-4802–3p, hsa-miR-23b-5p, hsa-miR-363–5p, hsa-miR-448, hsa-miR-4420, and hsa-miR-744–3p, respectively.

3.7. Validation of predicted siRNAs & selection of the best probable siRNAs

siRNAPred was used to check the validity and effectivity of the predicted siRNA molecules and values greater than 1 are considered highly effective. Among 131 siRNA molecules, 29 siRNAs for orf1ab were found to be highly effective (value > 1). These 29 siRNA molecules were primarily selected for further analysis. Additionally, to substantiate predicted siRNAs, the i-Score Designer was used to check the concordance of the siRNAs from siRNAPred. The results were mostly similar in both cases (Table 3).

3.8. Probable siRNAs against ORF1ab of SARS CoV-2 predicted by RNA-RNA interaction

RNA structure webserver was used to visualize the possible folding and corresponding MFE of folding (Fig. 4). The positive values (value > 0) indicate better applicants as those molecules are less prone to folding. The values of the predicted siRNAs were in the range of 1.5–1.8. According to the guide strands' folding structure pattern, 10 siRNAs were selected, which showed unpaired terminal ends and less degree of folding. Furthermore, by using bifold section of RNA structure web server, the hybrid RNA structure of selected siRNAs and target sequences were predicted (Fig. 5) along with their corresponding MFE of hybridization (Table 3). Finally, based on GC percentage, T_m value, validity of siRNA, free energy, and folding, 10 of them were selected to be the highest probable siRNAs against the ORF1ab gene of SARS-CoV-2.

4. Discussion

Coronaviruses possess one of the biggest known genomes among the RNA viruses [67,68] that causes respiratory diseases in a wide variety of species including bats, birds, cats, dogs, pigs, mice, horses, whales, and humans. Till date, seven types of coronaviruses are found to be transmitted to the human population [69], and among them, SARS-CoV-2 has been proven to be the deadliest. The genome of SARS-CoV-2 contains ORF1ab gene that encodes orf1ab polyprotein which is responsible for the replication and transcription of viral RNAs [70]. This gene also encodes 16 non-structural proteins [9] that play a crucial role in deceiving the host immune system. The RNA sequence of ORF1ab is used in this study to predict the interfering RNA molecules against SARS-CoV-2.

Interfering RNAs are small non-coding RNAs that normally function in the negative regulation of a target mRNA expression at the post-transcriptional stage. In case of miRNA, a partial complementarity (2–7 bp long) is enough for blocking translation. On the other hand, a full complementarity of the 3′ untranslated region (UTR) of an mRNA and the seed region of siRNAs results in effective silencing of gene expression [71]. Both miRNAs and siRNAs play significant roles in many key biological processes such as cell growth, tissue differentiation, cell proliferation, embryonic development, and apoptosis [72]. Aberrations

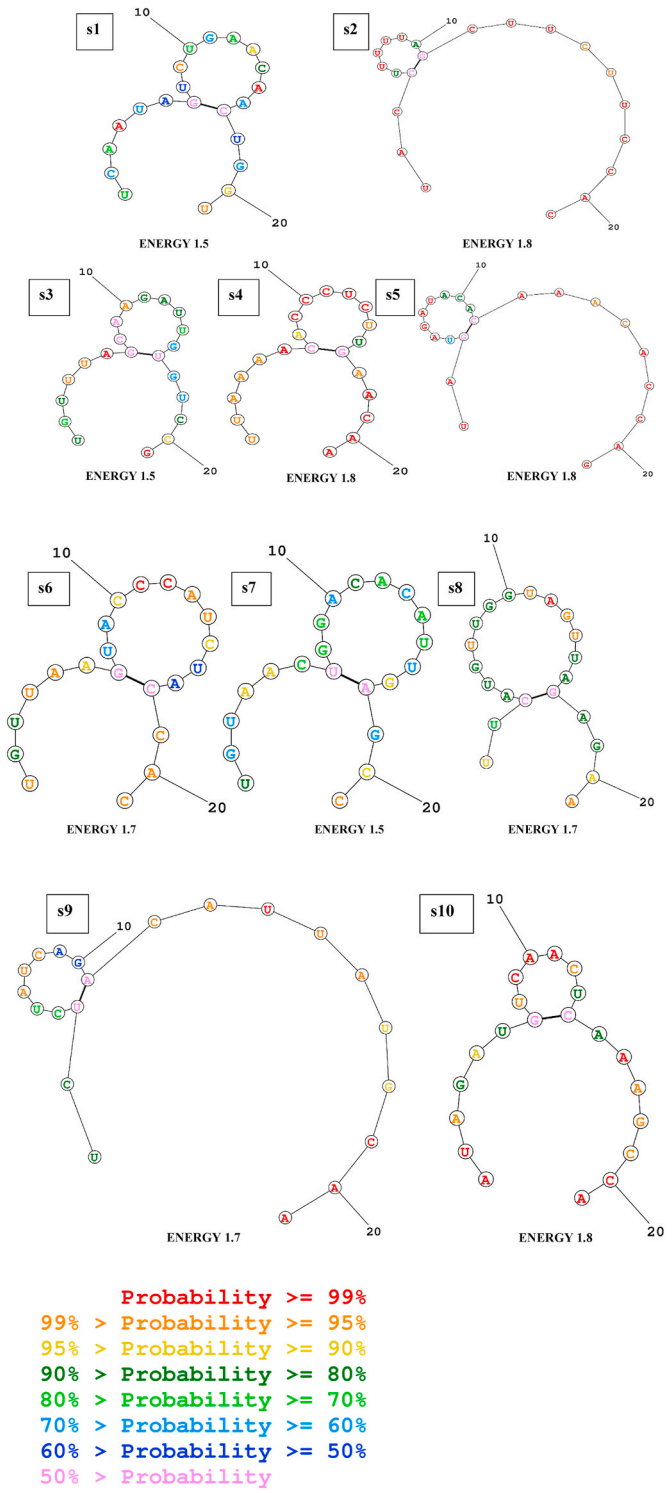

Fig. 4. Representation of the predicted siRNA guide strand's secondary structures with possible folding and minimum free energy values against ORF1ab sequence of SARS-CoV-2 respectively, s1. UCAAUAGUCUGAACAACUGG, s2. UACCUUUUUAGCUUCUUCCAC, s3. UGUUUAGCAAGAUUGUGUCC, s4. UUAAAACACCCUCUUGAACA, s5. UAGUAGAUACACAAACACCAG, s6. UGUUAAGUACCCAUCUACCAC, s7. UGUAACUGGACACAUUGAGCC, s8. UUCAUGUUGGUAGUUAGAGAA, s9. UCUCUAUCAGACAUUAUGCAA, and s10. AUAGAUGUCAACUCAAAGCCA. The siRNAs are in symmetry with the information provided in Table 3.

in the functionalities of these RNAs have already been linked to various diseases such as cancers [72,73], cardiovascular disease [74,75], schizophrenia [76,77], and psoriasis [78].

Now-a-days, researches are being focused on harnessing the mechanism of gene silencing by miRNAs and siRNAs in treating diseases including cancer [79] and cardiovascular disorders [80]. Based on the insights from these researches, we have utilized several bioinformatic tools to predict miRNA-based therapeutics against SARS-CoV-2. To determine effective and target-specific miRNA, ORF1ab gene sequence was initially analyzed by the VMIir analyzer, where 24 pre-miRNA hairpins were found. These pre-miRNAs are classified as MD or MR based on the direction (forward or reverse) of cleavage by endonuclease. The MD is categorized for functionally active miRNA duplexes that are cleaved by the RNase III Endonuclease Dicer from the 5′ end of pre-miRNA. On the other hand, the MR is categorized for functionally active miRNA duplexes that are cleaved by the same enzyme but from the 3′ end of pre-miRNA. For any given pre-miRNA, the proportion of forward or reverse miRNA strand loaded on the Argonaute protein depends mostly on the cell type or cellular environment [81,82]. Among the 24 pre-miRNA hairpins, 12 were found to meet the standard relying on significant sequence similarity with all human miRNA, as shown in Table 1.

Partial alignment of miRNAs seed region (2–7 bp) located at the 3′ UTR of the candidate miRNA precursor has been found to be significant during gene silencing [51]. Based on the sequence similarity of sorted miRNA precursor molecules with the host miRNA sequences, these can be utilized to predict the antiviral therapeutics against SARS-CoV-2 infection. Theoretically, the human miRNAs should have the capability of potentially silencing corresponding viral genes by binding specific sequences of mRNA. As the human (host) miRNAs can endogenously silence corresponding genes by post-transcriptional mRNA attenuation, their agomiR (selected similar sequenced miRNA precursors) will also be able to silence the gene expression in an exogenous pathway.

In this study, all the selected pre-miRNA hairpins contain GC content within 33.94%–45.21% determined by the GC content calculator. GC-rich target sites were avoided while selecting miRNAs to reduce the potential chance of self-secondary structure formation. Alongside the minimal free energy of hybridization, hybridization between the potential viral precursor miRNAs and the complementary template of the potential human miRNAs was determined where the most significant binding was observed (Table 2). Finally, after three steps of filtration (minimal free energy, GC content and significant hybridization), only 8 miRNA precursors from the 12 persisted. The qualified eight miRNAs from MD7, MD18, MD55, MD64, MD66, MD70, MR33, and MR43 hairpins would be the best candidate for targeting human cellular miRNAs where hairpin MD55 exhibited significant sequence similarity with hsa-miR-548b-5p, hsa-miR-624–5p, hsa-miR-4640–5p. hsa-miR-624–5p is located at human chromosome 14q12 [74,83], which imparts therapeutic relevance. hsa-miR-624–5p can inhibit the growth of hepatoblastoma cells *in vitro* [84] and also act as virus-detecting biomarkers [85]. The other 7 miRNA precursors also showed interaction with another 9 human miRNAs, respectively as shown in Table 2, and can play a significant role in host-pathogen interaction.

However, the frequency of miRNA expression across human tissues is not the same [86]. There are more than two thousand miRNAs in the human genome always expressing in different tissues in different amounts and maintaining the gene expressions [20]. Although miRNAs are endogenous regulatory noncoding RNA molecules, it is already known that miRNA can also be delivered into target cell exogenously for inducing their corresponding functions via agomiR delivery mechanisms if the endogenous miRNA expression is too low [87]. Thereby, because of having all the necessary characteristics to silence the ORF1ab gene, the predicted human miRNAs or their agomiRs will be able to function as potential antivirals against COVID-19.

As mentioned above, siRNA stipulates supreme complementarity

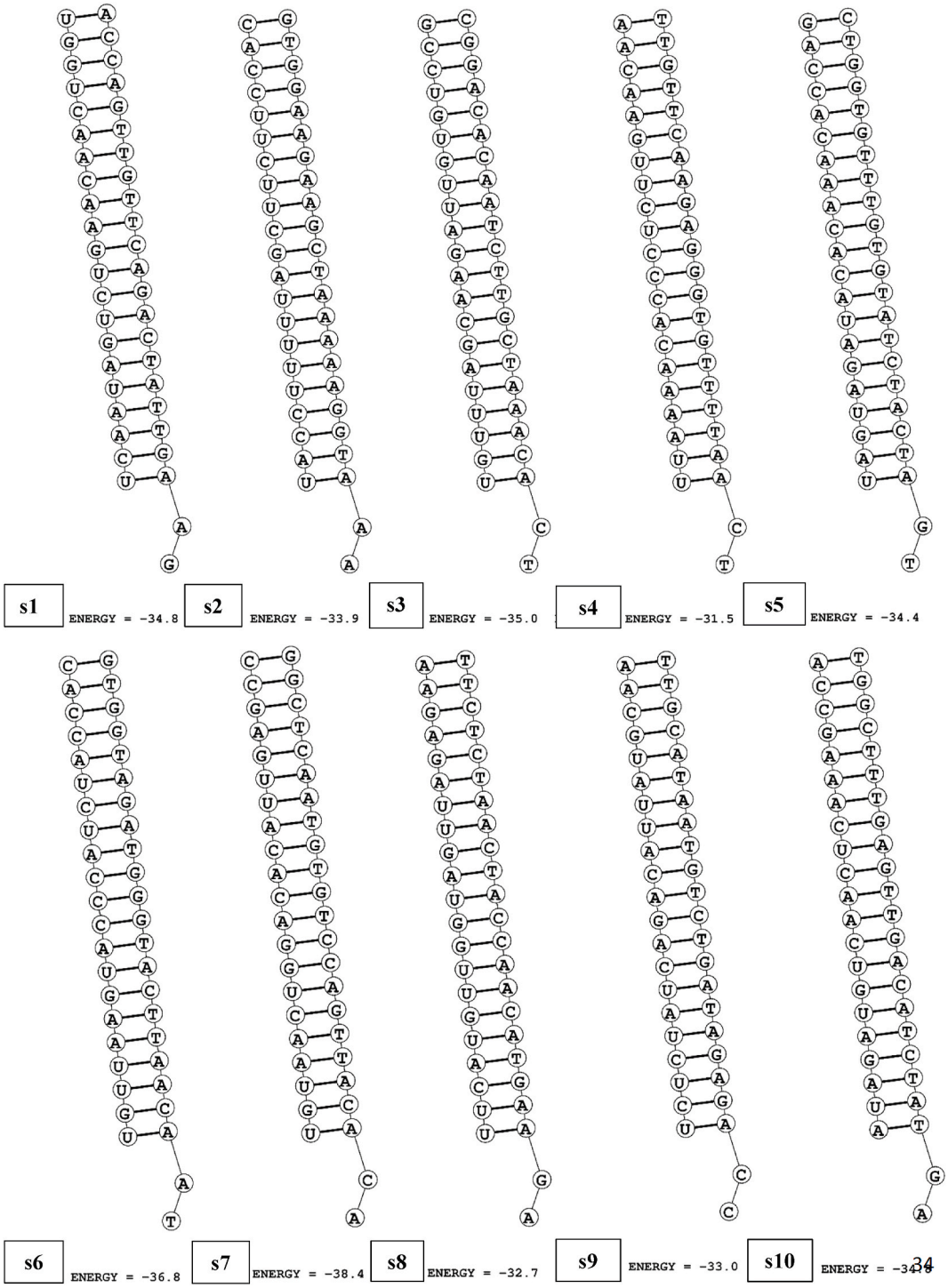

Fig. 5. Secondary structures of potential target–siRNA duplex of SARS-CoV-2.

between the siRNA guide strand and the extremely specific target mRNA. Transcripts possess complementarity to the 7-nucleotides seed region where siRNA could down-regulate unintended genes in a growing body. Therefore, off-target gene silencing may often provide incongruous binding that leads to misinterpretation. Thus, siDirect 2.0 software utilizes an efficient algorithm for designing functional siRNAs with a minimal off-target effect based on the mechanistic features that are considered for the value of mammalian RNAi. On the other hand, the seed-dependent off-target effect is highly correlated to the thermodynamic stability of the duplex formation [57]. The T_m of the seed-target duplex exhibits a strong positive correlation with the induction of seed-dependent off-target effects, which suggested that the T_m of 21.5 °C (Table 4) may serve as the benchmark to discriminate the almost off-target-free seed sequences from the off-target-positive ones [54]. Still, the BLASTn similarity searches from NCBI were used to verify the off-target where all predicted siRNAs were subjected to BLASTn. Here, a total of 131 siRNA molecules for the ORF1ab gene of SARS CoV-2 were used for further analysis with different parameters to determine their perfection.

GC content of the siRNA duplex is one of the crucial parameters that may affect siRNA functionality and the strongest correlation between siRNA functionality and GC content was observed [88]. For putative

Table 4
T_m values of predicted siRNA (guide strand and passenger strand).

RNA oligo sequences 21 nt guide (5′→3′) 21 nt passenger (5′→3′)	Seed-duplex stability (T_m)°C	
	Guide	Passenger
UCAAUAGUCUGAACAACUGGU CAGUUGUUCAGACUAUUGAAG	11.6 °C	17.8 °C
UACCUUUUUAGCUUCUUCCAC GGAAGAAGCUAAAAAGGUAAA	17.3 °C	19.1 °C
UGUUUAGCAAGAUUGUGUCCG GACACAAUCUUGCUAAACACU	20.9 °C	19.3 °C
UUAAAACACCCUCUUGAACAA GUUCAAGAGGGUGUUUUAACU	7.2 °C	20.4 °C
UAGUAGAUACACAAACACCAG GGUGUUUGUGUAUCUACUAGU	18.9 °C	19.3 °C
UGUUAAGUACCCAUCUACCAC GGUAGAUGGGUACUUAACAAU	12.9 °C	20.3 °C
UGUAACUGGACACAUUGAGCC CUCAAUGUGUCCAGUUACACA	19.0 °C	20.5 °C
UUCAUGUUGGUAGUUAGAGAA CUCUAACUACCAACAUGAAGA	20.5 °C	18.9 °C
UCUCUAUCAGACAUUAUGCAA GCAUAAUGUCUGAUAGAGACC	20.2 °C	5.6 °C
AUAGAUGUCAACUCAAAGCCA GCUUUGAGUUGACAUCUAUGA	20.3 °C	16.6 °C

helicase that is tentatively associated with the RISC [89] complex [21] and a prohibitive secondary structure of the target, mRNA may slow down siRNA duplex unwinding because of too high GC content. However, too low GC content may reduce the efficiency of target mRNA recognition and hybridization. In our study, all the selected siRNA molecules held GC content within 33.33%–47.62% determined by the GC content calculator, which is within a suitable range that supports the feasibility of those siRNAs [55]. Thus, our predicted siRNA duplex has been optimized by testifying through various parameters to be stable structurally.

In the heat capacity plot, the C_p is plotted as a function of temperature and when the C_p is a function of T_m, it is indicated as T_mC_p. The local maximum of the heat capacity curve defines the T_mC_p. Similarly, when the mole fractions are plotted as a function of temperature, it resembles a concentration plot, and with T_m it is indicated as T_m(Conc). T_m(Conc) is the point at which the concentration of the double-stranded molecule is one-half of its maximum value [61]. The entire equilibrium melting profiles were estimated by the DNAMelt web server as a function of temperature. Here, the higher the T_mC_p and T_m(Conc) values, the better the RNAi molecules are, and our predicted miRNA and siRNAs showed high melting profiles, as shown in Tables 1 and 3 In addition, the validations of primarily selected siRNA molecules were analyzed by siRNAPred to understand the efficacy of a siRNA with respect to inhibition of its target mRNA. In this case, 10 potential siRNA molecules were predicted to be potential antiviral candidates due to their high validity score (value $\geq$ 1) (Table 3). For the further assurance of this validation result, another software, the i-Score Designer was used, and it gave satisfactory results by s-Biopredsi score and i-Score using second-generation algorithms. These two scores showed that the predicted siRNAs had genuine scores that imparted from 80% to more than 90% effective functioning except two siRNAs, the S6 and S7 [64] and these scores are given in Table 3. This tool has also anticipated a nearly similar competence ranking for the predicted siRNAs. Since results have been found convenient using two different prediction tools that use different methodologies, it can be concluded that the predicted siRNAs have been reached into a significant level to be called “validated”.

Another way to determine the function of RNAi is molecular structure building by computational methods [90], and these computational methods of modeling RNA secondary structure have been proven to be valuable in many cases in which crystal structures are not available [91]. Alongside RNA’s molecular structure prediction, MFE is also considered as an accuracy benchmark [92]. The negative free energy value is more useful in this regard, and it explains the strong binding of the predicted RNAi with the target site [93]. In our current study, hybridization and minimal free energy of binding were predicted using the RNAhybrid webserver for miRNAs and bifold section of RNA structure webserver for siRNAs. Free energy of binding with target of predicted potential miRNA molecules are ranged from −10 kcal/mol to −17.2 kcal/mol (Table 2) and siRNA molecules are −34.80, −33.90, −35.00, −31.50, −34.40, −36.80, −38.40, −32.70, −33.00, and −34.80 kcal/mol (Table 3) and their respective RNA-RNA secondary structures are shown in Fig. 5.

In RNAi, guide RNAs direct RISC to their mRNA targets, thus enabling the cleavage that leads to gene silencing. The least the degree of guide-RNA secondary structure formation, the strongest the gene silencing by siRNA. Because an unstructured guide strand can mediate the efficient silencing of mRNA by binding with it, whereas base-paired terminals of the guide strand make the siRNA inactive and least available to bind with the complementary mRNA [94]. In this analysis, this method’s results predicted the secondary structure of siRNAs, as shown in Fig. 4. These predicted siRNAs of this analysis also showed terminal nucleotides’ availability in guide RNA structures and less degree of folding of guide RNAs. These criteria determine a strong silencing of targeted mRNAs by the selected siRNA guide strands. It is now well-documented that siRNA is comparatively better than miRNA due to its maximum sequence similarity that exert high affinity towards target mRNA and favorable delivery techniques (via lipid-based transfection, nanoparticle, etc.) into the cell [95]. Thus, it can be concluded that they are the best candidates as potential antiviral therapeutics for SARS-CoV-2.

Since this study solely represents in-silico drug development procedure as a predicted proof of concept rather than wet-lab analysis, further *in vitro and in vivo* studies must be done to confirm the actual efficacy and role of the predicted miRNAs and siRNAs in suppressing the ORF1ab gene of SARS-CoV-2.

5. Conclusion

In this study, several siRNA and miRNA molecules for silencing specific genes in SARS-CoV-2. Out of an array of potential candidates, 10 siRNA and 12 human miRNA molecules were predicted against SARS-CoV-2 as effective using all maximum parameters in optimum conditions. This study can be a starting point for the development of a novel antiviral therapy against SARS-CoV-2.

Declaration of competing interest

The authors declare no conflict of interest among them.

Acknowledgement

The authors would like to acknowledge the Department of Biochemistry and Molecular Biology, Shahjalal University of Science and Technology, Sylhet for laboratory facilities and logistic supports.

Appendix A. Supplementary data

Supplementary data to this article can be found online at https://doi.org/10.1016/j.imu.2021.100569.

References

[1] Wang C, Horby PW, Hayden FG, Gao GF. A novel coronavirus outbreak of global health concern. Lancet 2020;395:470–3. https://doi.org/10.1016/S0140-6736(20)30185-9.
[2] Wu F, Zhao S, Yu B, Chen Y-M, Wang W, Song Z-G, et al. A new coronavirus associated with human respiratory disease in China. Nature 2020;579:265–9. https://doi.org/10.1038/s41586-020-2008-3.
[3] Mahase E. Coronavirus: covid-19 has killed more people than SARS and MERS combined, despite lower case fatality rate. BMJ 2020;368. https://doi.org/10.1136/bmj.m641.

[4] WHO Coronavirus (COVID-19) Dashboard n.d. https://covid19.who.int (accessed March 26, 2021).

[5] Davies NG, Abbott S, Barnard RC, Jarvis CI, Kucharski AJ, Munday JD, et al. Estimated transmissibility and impact of SARS-CoV-2 lineage B.1.1.7 in England. MedRxiv 2021:2020. https://doi.org/10.1101/2020.12.24.20248822. 12.24.20248822.

[6] Chen RE, Zhang X, Case JB, Winkler ES, Liu Y, VanBlargan LA, et al. Resistance of SARS-CoV-2 variants to neutralization by monoclonal and serum-derived polyclonal antibodies. Nat Med 2021:1–10. https://doi.org/10.1038/s41591-021-01294-w.

[7] Covid-19 vaccine effectiveness affected by variants n.d. https://www.pharmaceutical-technology.com/comment/covid-19-vaccine-effectiveness-affected-by-variants/ (accessed March 26, 2021).

[8] Madhi SA, Baillie V, Cutland CL, Voysey M, Koen AL, Fairlie L, et al. Efficacy of the ChAdOx1 nCoV-19 covid-19 vaccine against the B.1.351 variant. N Engl J Med 2021. https://doi.org/10.1056/NEJMoa2102214.

[9] Wu F, Zhao S, Yu B, Chen Y-M, Wang W, Hu Y, et al. Complete genome characterisation of a novel coronavirus associated with severe human respiratory disease in Wuhan, China. BioRxiv 2020. https://doi.org/10.1101/2020.01.24.919183. 2020.01.24.919183.

[10] Cyranoski D. Profile of a killer: the complex biology powering the coronavirus pandemic. Nature 2020;581:22–6. https://doi.org/10.1038/d41586-020-01315-7.

[11] Prajapat M, Sarma P, Shekhar N, Avti P, Sinha S, Kaur H, et al. Drug targets for corona virus: a systematic review. Indian J Pharmacol 2020;52:56. https://doi.org/10.4103/ijp.IJP_115_20.

[12] Rosas-Lemus M, Minasov G, Shuvalova L, Inniss NL, Kiryukhina O, Brunzelle J, et al. High-resolution structures of the SARS-CoV-2 2′-O-methyltransferase reveal strategies for structure-based inhibitor design. Sci Signal 2020;13. https://doi.org/10.1126/scisignal.abe1202.

[13] Vuong W, Khan MB, Fischer C, Arutyunova E, Lamer T, Shields J, et al. Feline coronavirus drug inhibits the main protease of SARS-CoV-2 and blocks virus replication. Nat Commun 2020;11:4282. https://doi.org/10.1038/s41467-020-18096-2.

[14] Caplen NJ, Parrish S, Imani F, Fire A, Morgan RA. Specific inhibition of gene expression by small double-stranded RNAs in invertebrate and vertebrate systems. Proc Natl Acad Sci Unit States Am 2001;98:9742–7. https://doi.org/10.1073/pnas.171251798.

[15] Elbashir SM, Harborth J, Lendeckel W, Yalcin A, Weber K, Tuschl T. Duplexes of 21-nucleotide RNAs mediate RNA interference in cultured mammalian cells. Nature 2001;411:494–8. https://doi.org/10.1038/35078107.

[16] Fire A, Xu S, Montgomery MK, Kostas SA, Driver SE, Mello CC. Potent and specific genetic interference by double-stranded RNA in Caenorhabditis elegans. Nature 1998;391:806–11. https://doi.org/10.1038/35888.

[17] Hannon GJ. RNA interference. Nature 2002;418:244–51. https://doi.org/10.1038/418244a.

[18] McManus MT, Sharp PA. Gene silencing in mammals by small interfering RNAs. Nat Rev Genet 2002;3:737–47. https://doi.org/10.1038/nrg908.

[19] Bernstein E, Caudy AA, Hammond SM, Hannon GJ. Role for a bidentate ribonuclease in the initiation step of RNA interference. Nature 2001;409:363–6. https://doi.org/10.1038/35053110.

[20] Hammond SM. An overview of microRNAs. Adv Drug Deliv Rev 2015;87:3–14. https://doi.org/10.1016/j.addr.2015.05.001.

[21] Ishizuka A, Siomi MC, Siomi H. A Drosophila fragile X protein interacts with components of RNAi and ribosomal proteins. Genes Dev 2002;16:2497–508. https://doi.org/10.1101/gad.1022002.

[22] Martinez J, Patkaniowska A, Urlaub H, Lührmann R, Tuschl T. Single-stranded antisense siRNAs guide target RNA cleavage in RNAi. Cell 2002;110:563–74. https://doi.org/10.1016/S0092-8674(02)00908-X.

[23] Jackson AL, Linsley PS. Recognizing and avoiding siRNA off-target effects for target identification and therapeutic application. Nat Rev Drug Discov 2010;9:57–67. https://doi.org/10.1038/nrd3010.

[24] Nykänen A, Haley B, Zamore PD. ATP requirements and small interfering RNA structure in the RNA interference pathway. Cell 2001;107:309–21. https://doi.org/10.1016/S0092-8674(01)00547-5.

[25] Tétreault N, De Guire V. miRNAs: their discovery, biogenesis and mechanism of action. Clin Biochem 2013;46:842–5. https://doi.org/10.1016/j.clinbiochem.2013.02.009.

[26] Carthew RW, Sontheimer EJ. Origins and Mechanisms of miRNAs and siRNAs. Cell 2009;136:642–55. https://doi.org/10.1016/j.cell.2009.01.035.

[27] Kanasty R, Dorkin JR, Vegas A, Anderson D. Delivery materials for siRNA therapeutics. Nat Mater 2013;12:967–77. https://doi.org/10.1038/nmat3765.

[28] Morris KV. siRNA-mediated transcriptional gene silencing: the potential mechanism and a possible role in the histone code. Cell Mol Life Sci CMLS 2005;62:3057–66. https://doi.org/10.1007/s00018-005-5182-4.

[29] Ahluwalia JK, Khan SZ, Soni K, Rawat P, Gupta A, Hariharan M, et al. Human cellular microRNA hsa-miR-29a interferes with viral nef protein expression and HIV-1 replication. Retrovirology 2008;5:117. https://doi.org/10.1186/1742-4690-5-117.

[30] Park W-S, Hayafune M, Miyano-Kurosaki N, Takaku H. Specific HIV-1 env gene silencing by small interfering RNAs in human peripheral blood mononuclear cells. Gene Ther 2003;10:2046–50. https://doi.org/10.1038/sj.gt.3302099.

[31] Sanghvi VR, Steel LF. RNA silencing as a cellular defense against HIV-1 infection: progress and issues. Faseb J 2012;26:3937–45. https://doi.org/10.1096/fj.12-210765.

[32] Alhoot MA, Wang SM, Sekaran SD. Inhibition of dengue virus entry and multiplication into monocytes using RNA interference. PLoS Neglected Trop Dis 2011;5:e1410. https://doi.org/10.1371/journal.pntd.0001410.

[33] Escalera-Cueto M, Medina-Martínez I, del Angel RM, Berumen-Campos J, Gutiérrez-Escolano AL, Yocupicio-Monroy M. Let-7c overexpression inhibits dengue virus replication in human hepatoma Huh-7 cells. Virus Res 2015;196:105–12. https://doi.org/10.1016/j.virusres.2014.11.010.

[34] Ge Q, McManus MT, Nguyen T, Shen C-H, Sharp PA, Eisen HN, et al. RNA interference of influenza virus production by directly targeting mRNA for degradation and indirectly inhibiting all viral RNA transcription. Proc Natl Acad Sci Unit States Am 2003;100:2718–23. https://doi.org/10.1073/pnas.0437841100.

[35] Peng S, Wang J, Wei S, Li C, Zhou K, Hu J, et al. Endogenous cellular MicroRNAs mediate antiviral defense against influenza A virus. Mol Ther Nucleic Acids 2018;10:361–75. https://doi.org/10.1016/j.omtn.2017.12.016.

[36] Zhang H, Li Z, Li Y, Liu Y, Liu J, Li X, et al. A computational method for predicting regulation of human microRNAs on the influenza virus genome. BMC Syst Biol 2013;7:S3. https://doi.org/10.1186/1752-0509-7-S2-S3.

[37] Janssen HLA, Reesink HW, Lawitz EJ, Zeuzem S, Rodriguez-Torres M, Patel K, et al. Treatment of HCV infection by targeting MicroRNA. N Engl J Med 2013;368:1685–94. https://doi.org/10.1056/NEJMoa1209026.

[38] Korf M, Jarczak D, Beger C, Manns MP, Krüger M. Inhibition of hepatitis C virus translation and subgenomic replication by siRNAs directed against highly conserved HCV sequence and cellular HCV cofactors. J Hepatol 2005;43:225–34. https://doi.org/10.1016/j.jhep.2005.02.046.

[39] Pedersen IM, Cheng G, Wieland S, Volinia S, Croce CM, Chisari FV, et al. Interferon modulation of cellular microRNAs as an antiviral mechanism. Nature 2007;449:919–22. https://doi.org/10.1038/nature06205.

[40] Giulietti M, Righetti A, Cianfruglia L, Šabanović B, Armeni T, Principato G, et al. To accelerate the Zika beat: candidate design for RNA interference-based therapy. Virus Res 2018;255:133–40. https://doi.org/10.1016/j.virusres.2018.07.010.

[41] Uludağ H, Parent K, Aliabadi HM, Haddadi A. Prospects for RNAi therapy of COVID-19. Front Bioeng Biotechnol 2020;8. https://doi.org/10.3389/fbioe.2020.00916.

[42] Singh S, Gupta SK, Nischal A, Khattri S, Nath R, Pant KK, et al. Design of potential siRNA molecules for hepatitis delta virus gene silencing. Bioinformation 2012;8:749–57. https://doi.org/10.6026/97320630008749.

[43] Bumcrot D, Manoharan M, Koteliansky V, Sah DWY. RNAi therapeutics: a potential new class of pharmaceutical drugs. Nat Chem Biol 2006;2:711–9. https://doi.org/10.1038/nchembio839.

[44] Setten RL, Rossi JJ, Han S. The current state and future directions of RNAi-based therapeutics. Nat Rev Drug Discov 2019;18:421–46. https://doi.org/10.1038/s41573-019-0017-4.

[45] Grundhoff A. Computational prediction of viral miRNAs. In: van Rij RP, editor. Antivir. RNAi concepts methods appl. Totowa, NJ: Humana Press; 2011. p. 143–52. https://doi.org/10.1007/978-1-61779-037-9_8.

[46] Nur Suza Mohammad. An in silico approach to design potential siRNA molecules for ICP22 (US1) gene silencing of different strains of human herpes simplex 1. J Young Pharm 2013;5:46–9. https://doi.org/10.1016/j.jyp.2013.05.001.

[47] Nur SM, Hasan MdA, Amin MA, Hossain M, Sharmin T. Design of potential RNAi (miRNA and siRNA) molecules for Middle East respiratory syndrome coronavirus (MERS-CoV) gene silencing by computational method. Interdiscipl Sci Comput Life Sci 2015;7:257–65. https://doi.org/10.1007/s12539-015-0266-9.

[48] Mack GS. Erratum: MicroRNA gets down to business. Nat Biotechnol 2011;29. https://doi.org/10.1038/nbt0511-459a. 459–459.

[49] Grundhoff A, Sullivan CS, Ganem D. A combined computational and microarray-based approach identifies novel microRNAs encoded by human gamma-herpesviruses. RNA 2006;12:733–50. https://doi.org/10.1261/rna.2326106.

[50] Sullivan CS, Grundhoff A. Identification of viral microRNAs. Methods Enzymol 2007;427:3–23. https://doi.org/10.1016/S0076-6879(07)27001-6.

[51] Hasan MM, Akter R, Ullah MS, Abedin MJ, Ullah GMA, Hossain MZ. A computational approach for predicting role of human microRNAs in MERS-CoV genome. Adv Bioinforma 2015.

[52] Griffiths-Jones S, Grocock RJ, van Dongen S, Bateman A, Enright AJ. miRBase: microRNA sequences, targets and gene nomenclature. Nucleic Acids Res 2006;34:D140–4. https://doi.org/10.1093/nar/gkj112.

[53] Kozomara A, Griffiths-Jones S. miRBase: annotating high confidence microRNAs using deep sequencing data. Nucleic Acids Res 2014;42:D68–73. https://doi.org/10.1093/nar/gkt1181.

[54] Naito Y, Yoshimura J, Morishita S, Ui-Tei K. siDirect 2.0: updated software for designing functional siRNA with reduced seed-dependent off-target effect. BMC Bioinf 2009;10:392. https://doi.org/10.1186/1471-2105-10-392.

[55] Amarzguioui M, Prydz H. An algorithm for selection of functional siRNA sequences. Biochem Biophys Res Commun 2004;316:1050–8. https://doi.org/10.1016/j.bbrc.2004.02.157.

[56] Lander ES, Linton LM, Birren B, Nusbaum C, Zody MC, Baldwin J, et al. Initial sequencing and analysis of the human genome. Nature 2001;409:860–921. https://doi.org/10.1038/35057062.

[57] Ui-Tei K, Naito Y, Nishi K, Juni A, Saigo K. Thermodynamic stability and Watson–Crick base pairing in the seed duplex are major determinants of the efficiency of the siRNA-based off-target effect. Nucleic Acids Res 2008;36. https://doi.org/10.1093/nar/gkn902. 7100–9.

[58] Ui-Tei K, Naito Y, Takahashi F, Haraguchi T, Ohki-Hamazaki H, Juni A, et al. Guidelines for the selection of highly effective siRNA sequences for mammalian and chick RNA interference. Nucleic Acids Res 2004;32:936–48. https://doi.org/10.1093/nar/gkh247.

[59] Reynolds A, Leake D, Boese Q, Scaringe S, Marshall WS, Khvorova A. Rational siRNA design for RNA interference. Nat Biotechnol 2004;22:326–30. https://doi.org/10.1038/nbt936.
[60] Bernhart SH, Tafer H, Mückstein U, Flamm C, Stadler PF, Hofacker IL. Partition function and base pairing probabilities of RNA heterodimers. Algorithm Mol Biol 2006;1:3. https://doi.org/10.1186/1748-7188-1-3.
[61] Markham NR, Zuker M. DINAMelt web server for nucleic acid melting prediction. Nucleic Acids Res 2005;33:W577–81. https://doi.org/10.1093/nar/gki591.
[62] Krüger J, Rehmsmeier M. RNAhybrid: microRNA target prediction easy, fast and flexible. Nucleic Acids Res 2006;34:W451–4. https://doi.org/10.1093/nar/gkl243.
[63] Rehmsmeier M, Steffen P, Höchsmann M, Giegerich R. Fast and effective prediction of microRNA/target duplexes. RNA 2004;10:1507–17. https://doi.org/10.1261/rna.5248604.
[64] Ichihara M, Murakumo Y, Masuda A, Matsuura T, Asai N, Jijiwa M, et al. Thermodynamic instability of siRNA duplex is a prerequisite for dependable prediction of siRNA activities. Nucleic Acids Res 2007;35. https://doi.org/10.1093/nar/gkm699. e123–e123.
[65] Lu ZJ, Gloor JW, Mathews DH. Improved RNA secondary structure prediction by maximizing expected pair accuracy. RNA 2009;15:1805–13. https://doi.org/10.1261/rna.1643609.
[66] Bellaousov S, Reuter JS, Seetin MG, Mathews DH. RNAstructure: web servers for RNA secondary structure prediction and analysis. Nucleic Acids Res 2013;41:W471–4. https://doi.org/10.1093/nar/gkt290.
[67] Gorbalenya AE, Enjuanes L, Ziebuhr J, Snijder EJ. Nidovirales: evolving the largest RNA virus genome. Virus Res 2006;117:17–37. https://doi.org/10.1016/j.virusres.2006.01.017.
[68] Wertheim JO, Chu DKW, Peiris JSM, Pond SLK, Poon LLM. A case for the ancient origin of coronaviruses. J Virol 2013;87:7039–45. https://doi.org/10.1128/JVI.03273-12.
[69] Seah I, Agrawal R. Can the coronavirus disease 2019 (COVID-19) affect the eyes? A review of coronaviruses and ocular implications in humans and animals. Ocul Immunol Inflamm 2020;28:391–5. https://doi.org/10.1080/09273948.2020.1738501.
[70] Laha S, Chakraborty J, Das S, Manna SK, Biswas S, Chatterjee R. Characterizations of SARS-CoV-2 mutational profile, spike protein stability and viral transmission. Infect Genet Evol 2020;85:104445. https://doi.org/10.1016/j.meegid.2020.104445.
[71] Casal ML, Dambach DM, Meister T, Jezyk PF, Patterson DF, Henthorn PS. Familial glomerulonephropathy in the bullmastiff. Vet Pathol 2004;41:319–25. https://doi.org/10.1354/vp.41-4-319.
[72] Esquela-Kerscher A, Slack FJ. Oncomirs — microRNAs with a role in cancer. Nat Rev Canc 2006;6:259–69. https://doi.org/10.1038/nrc1840.
[73] Serban M, Ghiorghiu I, Craciunescu I, Calin C, Platon P, Apetrei E, et al. Spontaneous echo contrast of unexpected etiology. Eur J Echocardiogr 2006;7:257–9. https://doi.org/10.1016/j.euje.2005.05.007.
[74] Latronico Michael VG, Daniele Catalucci, Gianluigi Condorelli. Emerging role of MicroRNAs in cardiovascular biology. Circ Res 2007;101:1225–36. https://doi.org/10.1161/CIRCRESAHA.107.163147.
[75] Rooij E van, Sutherland LB, Qi X, Richardson JA, Hill J, Olson EN. Control of stress-dependent cardiac growth and gene expression by a MicroRNA. Science 2007;316:575–9. https://doi.org/10.1126/science.1139089.
[76] Hansen T, Olsen L, Lindow M, Jakobsen KD, Ullum H, Jonsson E, et al. Brain expressed microRNAs implicated in schizophrenia etiology. PloS One 2007;2:e873. https://doi.org/10.1371/journal.pone.0000873.
[77] Perkins DO, Jeffries CD, Jarskog LF, Thomson JM, Woods K, Newman MA, et al. microRNA expression in the prefrontal cortex of individuals with schizophrenia and schizoaffective disorder. Genome Biol 2007;8:R27. https://doi.org/10.1186/gb-2007-8-2-r27.
[78] Sonkoly E, Wei T, Janson PCJ, Sääf A, Lundeberg L, Tengvall-Linder M, et al. MicroRNAs: novel regulators involved in the pathogenesis of psoriasis? PloS One 2007;2:e610. https://doi.org/10.1371/journal.pone.0000610.
[79] Stahlhut C, Slack FJ. MicroRNAs and the cancer phenotype: profiling, signatures and clinical implications. Genome Med 2013;5:111. https://doi.org/10.1186/gm516.
[80] Harada Masahide, Luo Xiaobin, Toyoaki Murohara, Yang Baofeng, Dobromir Dobrev, Stanley Nattel. MicroRNA regulation and cardiac calcium signaling. Circ Res 2014;114:689–705. https://doi.org/10.1161/CIRCRESAHA.114.301798.
[81] Yoda M, Kawamata T, Paroo Z, Ye X, Iwasaki S, Liu Q, et al. ATP-dependent human RISC assembly pathways. Nat Struct Mol Biol 2010;17:17–23. https://doi.org/10.1038/nsmb.1733.
[82] Meijer HA, Smith EM, Bushell M. Regulation of miRNA strand selection: follow the leader? Biochem Soc Trans 2014;42:1135–40. https://doi.org/10.1042/BST20140142.
[83] Gardiner E, Carroll A, Tooney PA, Cairns MJ. Antipsychotic drug-associated gene–miRNA interaction in T-lymphocytes. Int J Neuropsychopharmacol 2014;17:929–43. https://doi.org/10.1017/S1461145713001752.
[84] Rahman A, Zaman K, Topics in anti-cancer research. https://www.eurekaselect.com/177919/volume/8. accessed February 8, 2021.
[85] Zhang S, Ouyang X, Jiang X, Gu D, Lin Y, Kong SK, et al. Dysregulated serum MicroRNA expression profile and potential biomarkers in hepatitis C virus-infected patients. Int J Med Sci 2015;12:590–8. https://doi.org/10.7150/ijms.11525.
[86] Ludwig N, Leidinger P, Becker K, Backes C, Fehlmann T, Pallasch C, et al. Distribution of miRNA expression across human tissues. Nucleic Acids Res 2016;44:3865–77. https://doi.org/10.1093/nar/gkw116.
[87] Wang Z. The guideline of the design and validation of MiRNA mimics. In: Wu W, editor. MicroRNA cancer methods protoc. Totowa, NJ: Humana Press; 2011. p. 211–23. https://doi.org/10.1007/978-1-60761-863-8_15.
[88] Chan CY, Carmack CS, Long DD, Maliyekkel A, Shao Y, Roninson IB, et al. A structural interpretation of the effect of GC-content on efficiency of RNA interference. BMC Bioinf 2009;10:S33. https://doi.org/10.1186/1471-2105-10-S1-S33.
[89] Zhang S, Ouyang X, Jiang X, Gu D, Lin Y, Kong SK, et al. Dysregulated serum MicroRNA expression profile and potential biomarkers in hepatitis C virus-infected patients. Int J Med Sci 2015;12:590–8. https://doi.org/10.7150/ijms.11525.
[90] Hajiaghayi M, Condon A, Hoos HH. Analysis of energy-based algorithms for RNA secondary structure prediction. BMC Bioinf 2012;13:22. https://doi.org/10.1186/1471-2105-13-22.
[91] Ding Y, Chan CY, Lawrence CE. RNA secondary structure prediction by centroids in a Boltzmann weighted ensemble. RNA 2005;11:1157–66. https://doi.org/10.1261/rna.2500605.
[92] Mathews DH. Predicting a set of minimal free energy RNA secondary structures common to two sequences. Bioinformatics 2005;21:2246–53. https://doi.org/10.1093/bioinformatics/bti349.
[93] Mückstein U, Tafer H, Hackermüller J, Bernhart SH, Stadler PF, Hofacker IL. Thermodynamics of RNA–RNA binding. Bioinformatics 2006;22:1177–82. https://doi.org/10.1093/bioinformatics/btl024.
[94] Patzel V, Rutz S, Dietrich I, Köberle C, Scheffold A, Kaufmann SHE. Design of siRNAs producing unstructured guide-RNAs results in improved RNA interference efficiency. Nat Biotechnol 2005;23:1440–4. https://doi.org/10.1038/nbt1151.
[95] Chen Y, Cheng G, Mahato RI. RNAi for treating hepatitis B viral infection. Pharm Res (N Y) 2008;25:72–86. https://doi.org/10.1007/s11095-007-9504-0.